HHS Public Access

Author manuscript

FASEB J. Author manuscript; available in PMC 2022 March 28.

Published in final edited form as:

FASEB J. 2021 December ; 35(12): e22066. doi:10.1096/fj.202101484R.

The effects of maturation and aging on the rotator cuff tendon-to-bone interface

Xiping Jiang[a,b,c], **Melinda Wojtkiewicz**[d], **Chinmay Patwardhan**[e], **Sydney Greer**[a,c], **Yunfan Kong**[a], **Mitchell Kuss**[a], **Xi Huang**[f], **Jun Liao**[e], **Yongfeng Lu**[f], **Andrew Dudley**[a,c], **Rebekah L. Gundry**[d], **Matthias Fuchs**[g], **Philipp Streubel**[h], **Bin Duan**[a,b,i,j,*]

[a]Mary & Dick Holland Regenerative Medicine Program, University of Nebraska Medical Center, Omaha, NE, 68198, USA

[b]Division of Cardiology, Department of Internal Medicine, University of Nebraska Medical Center, Omaha, NE, 68198, USA

[c]Molecular Genetics and Cell Biology Program; Department of Genetics, Cell Biology and Anatomy, University of Nebraska Medical Center, Omaha, NE, 68198, USA

[d]CardiOmics Program, Center for Heart and Vascular Research; Division of Cardiovascular Medicine; and Department of Cellular and Integrative Physiology, University of Nebraska Medical Center, Omaha, NE, 68198, USA

[e]Department of Bioengineering, University of Texas at Arlington, Arlington, TX, 76019, USA

[f]Department of Electrical and Computer Engineering, University of Nebraska-Lincoln, Lincoln, NE, 68588, USA

[g]Department of Physics and Astronomy, University of Nebraska-Lincoln, Lincoln, NE, 68588, USA

[h]Department of Orthopedic Surgery and Rehabilitation, University of Nebraska Medical Center, Omaha, NE, 68198, USA

[i]Department of Surgery, College of Medicine, University of Nebraska Medical Center, Omaha, NE, 68198, USA

[j]Department of Mechanical and Materials Engineering, University of Nebraska-Lincoln, Lincoln, NE, 68588, USA

Abstract

Rotator cuff tendon injuries often occur at the tendon-to-bone interface (i.e., enthesis) area, with a high prevalence for the elderly population, but the underlying reason for this phenomenon is still

*Corresponding author. Mailing address: University of Nebraska Medical Center, Bin Duan, DRC2 6014, 601 S Saddle Creek Road, Omaha NE 68106; bin.duan@unmc.edu (B. Duan); Phone number: 4025599637.

Author contributions

X. Jiang: performed research, analyzed data, and wrote paper; M. Wojtkiewicz: performed research and wrote paper; C. Patwardhan: performed research, analyzed data, and wrote paper; S. Greer: performed research; Y. Kong: performed research; M. Kuss: wrote paper; X. Huang: performed research and wrote paper; J. Liao: performed research and wrote paper; Y. Lu: performed research and wrote paper; A. Dudley: performed research; R. L. Gundry: performed research and wrote paper; M. Fuchs: designed research; P. Streubel: designed research; B. Duan: designed research and wrote paper.

Conflict of interest statement

The authors have stated explicitly that there are no conflicts of interest in connection with this article.

unknown. The objective of this study is to identify the histological, molecular, and biomechanical alterations of the rotator cuff enthesis with maturation and aging in a mouse model. Four different age groups of mice (newborn, young, adult, and old) were studied. Striking variations of the entheses were observed between newborn and other matured groups, with collagen content, proteoglycan deposition, collagen fiber dispersion significantly higher in the newborn group. The compositional and histological features of young, adult, and old groups did not show significant differences, except having increased proteoglycan deposition and thinner collagen fibers at the insertion sites in the old group. Nanoindentation testing showed that the old group had a smaller compressive modulus at the insertion site when compared with other groups. However, tensile mechanical testing reported that the old group demonstrated a significantly higher failure stress when compared with the young and adult groups. The proteomics analysis detected dramatic differences in protein content between newborn and young groups but minor changes among young, adult, and old groups. These results demonstrated: (1) the significant alterations of the enthesis composition and structure occur from the newborn to the young time period; (2) the increased risk of rotator cuff tendon injuries in the elderly population is not solely because of old age alone in the rodent model.

Keywords

enthesis; age; biomechanical properties; nanoindentation; proteomics

1. Introduction

Rotator cuff tendon injuries are among the most common musculoskeletal diseases and result in shoulder pain and joint disorders [1]. The injuries are associated with more than 4.5 million physician visits and 40,000 surgical treatments annually in the United States [2, 3]. The prevalence of rotator cuff injuries increases considerably with age [4]. Injuries occur in about 9.7% of people aged 20 years and younger, while it increases to 62% in people aged 80 years and older [5]. Despite improved instruments and surgical approaches, the retear rate of rotator cuff tears is ~7% for people of all age groups, and the retear rate for people over 70 years old reaches 25% [6, 7]. Although there is an apparent trend between the onset of rotator cuff injuries and aging, the underlying reason for this phenomenon is still unknown. Thus, an in-depth investigation of the native rotator cuff tendon-to-bone interface changes with the maturation and aging process is needed.

The rotator cuff consists of four muscles (subscapularis, supraspinatus, infraspinatus, and teres minor) that stabilize the shoulder joint. The tendon tissues attach to bone across a multi-tissue interface with spatial gradients in composition, structure, and mechanical properties [8-10]. The tendon-to-bone interface (i.e., enthesis) has four different zones in general (i.e., tendon, non-mineralized fibrocartilage, mineralized fibrocartilage, and bone). It can minimize the stress concentration and mediate load transfer between the soft and hard tissues [11]. Tenocytes populate the tendon zone, with linearly arrayed type I collagen fibers [12]. The fibrocartilage zone is populated by fibrochondrocytes, and is composed of types II and III collagen [13]. The mineralized fibrocartilage zone is occupied by hypertrophic fibrochondrocytes with mineralization. The major extracellular matrices (ECM) of the

mineralized fibrocartilage zone are type II and type X collagen [14]. The fourth zone consists of bone tissue, within which osteoblasts, osteocytes, and osteoclasts reside in a matrix of mineralized type I collagen [15]. Advanced glycation end (AGE) products are the formation of cross-links between collagen fibrils by the addition of sugars [16], correlating with the aging process of both tendon and bone tissues [17, 18]. The changes of AGE products at the tendon-to-bone interface with age are still unknown.

Currently, studies on the tendon-to-bone interface mainly focus on the development and healing of the enthesis [19-22]. Very few studies have investigated the effects of maturation and aging. For example, researchers found that the absence of muscle loading impaired the function of the enthesis during development, resulting in defects in mineral accumulation and fibrocartilage formation [23]. Plate et al. reported that compared to young rats, old ones had diminished tendon-to-bone healing after rotator cuff injury with decreased failure strength and collagen fiber organization [24]. Wang et al. used a bovine model with three age groups representing neonatal, immature, and mature to study the ligament-to-bone interface of the anterior cruciate ligament (ACL). They primarily illustrated the histological changes at the interface area, including extracellular matrix, collagen fiber orientation, cellularity, alkaline phosphatase (ALP) activity, and mineral distribution [25]. There are several limitations with the current studies. First, no study characterizes the property changes of the rotator cuff tendon-to-bone interface. Second, the mature group, with bovines at the ages of 2-5 years, in the previous studies is not old enough to represent the elder individuals in human beings [26, 27]. Third, previous studies only qualitatively evaluated the histological variations at the enthesis without quantitative biomechanical and molecular analyses. Fourth, the factor of sex was not considered in previous studies' designs. Thus, the effects of maturation and aging of the rotator cuff tendon-to-bone interface remains underexplored. A comprehensive understanding of the age-related changes at the enthesis will benefit both disease prevention and tissue regeneration.

Here, we conducted a systematic evaluation of the rotator cuff tendon-to-bone interface with respect to age at structural, molecular, and biomechanical levels. The overview of the study design is illustrated in Fig. 1. We used mice with four different age groups: newborn (day 0), young (2-3 months old), adult (6-8 months old), and old (15-18 months old). The old group of the mice represents humans at the ages of 60-65 years old [28]. Histological analyses were performed, including overall collagen and proteoglycan distribution, types (type I, II, and III collagen) and fiber thickness (thin and thick fibers) of collagen distribution, the receptor for advanced glycation end products (RAGE) deposition, and collagen fiber orientation. Analyses of extracellular matrix components, including collagen and glycosaminoglycan (GAG), and DNA contents were conducted. Laser captured microdissection (LCM) can precisely isolate the region of interest from tissue sections under the microscope and allows for the performance of downstream analysis [29, 30]. LCM has been applied for enthesis isolation of the postnatal mice [31, 32]. Kawamot's film method enables cryosection preparation of bone tissue samples without chemically fixation and decalcification, avoiding potential denaturation of proteins [33]. It also preserves the structure of the enthesis region after sectioning. We combined the LCM and Kawamot's film method to harvest the tendon-to-bone interface from the non-fixed and undecalcified cryosection samples of

all four groups, followed by proteomics analysis. For biomechanical analysis, both local compressive testing and bulk tensile testing of the tendon-to-bone interface were conducted.

2. Materials and methods

2.1. Animals and experimental groups

The research protocol and animal care were approved by the Institutional Animal Care and Use Committee (IACUC) at the University of Nebraska Medical Center (UNMC). Swiss Webster mice purchased from Charles River Laboratories were used for the experiment. These mice are from four different age groups: newborn (N, day 0), young (Y, 2-3 months old), adult (A, 6-8 months old), and old (O, 15-18 months old). Fifty-one newborn mice were used for the newborn group. For the young, adult, and old groups, each group had 36 mice with equal numbers of males and females.

2.2. Histological analysis

Six mice from each group were used to perform the histological analysis. For the young, adult, and old groups, equal numbers of males and females were used. For the newborn mice, the supraspinatus tendon with attached cartilage was dissected under a microscope. The supraspinatus muscle-tendon with attached humerus bone complexes from the other three age groups were also isolated. The harvested samples were fixed in buffered formalin, decalcified with Cal-Rite (Fisher Scientific, Hampton, NH, USA), routinely dehydrated, and paraffin-embedded. Sections of the embedded specimens, with 5μm thickness, were obtained along the long axis of the supraspinatus tendon. The sections were then treated with Hematoxylin and eosin (H&E) staining, Masson's trichrome (MT) staining, Safranin O (SO) staining, and picrosirius red (PR) staining. The stained slides were scanned at 40× magnification. The images of MT staining, SO staining, and PR staining were semi-quantitatively analyzed with ImageJ software (National Institutes of Health, USA). The blue staining area of five randomly selected 50 μm × 50 μm areas at the enthesis region from the MT staining were measured for each image. The proportions of collagen's area were expressed as the percentage of the blue stained area divided by the total area [34]. The metachromasia areas of five randomly selected 50 μm × 50 μm areas at the enthesis region from the SO staining were measured for each image. The proportion of metachromasia area was expressed as the percentage of the metachromasia area divided by the total area [35]. The orange and green stained areas within five randomly selected 50 μm × 50 μm areas at the enthesis region from the PR staining were measured for each image. The ratio of thin fibers / thick fibers was expressed as the percentage of the green-stained area divided by the orange-stained area [36, 37].

2.3. Immunohistochemistry (IHC) analysis

5-μm thick sections were deparaffinized with CitriSolv (Decon Labs, Inc., King of Prussia, PA, USA). These sections were then rehydrated by sequentially immersing them in ethanol with graded concentrations. The slides were treated with 10 mM sodium citrate buffer pH 6.0 (Sigma, St. Louis, MO, USA) in a 75°C water bath for antigen retrieval. Sections for collagen type I and RAGE staining were prepared with VECTASTAIN® ABC Kits (Vector Laboratories, Burlingame, CA, USA). Sections for collagen types II and III staining were

prepared with M.O.M.® (Mouse on Mouse) Immunodetection Kits (Vector Laboratories, Burlingame, CA, USA). The sections were then incubated with 3% hydrogen peroxide in methanol to deactivate the endogenous peroxidase and subsequently blocked with blocking serum. After that, the sections were incubated overnight at 4°C with an anti-collagen type I primary antibody (Col I, NB600-408, Novus Biologicals, Littleton, CO, USA), anti-collagen type II primary antibody (Col II, NB600-844, Novus Biologicals, Littleton, CO, USA), anti-collagen type III primary antibody (Col III, NBP1-05119, Novus Biologicals, Littleton, CO, USA), or anti-RAGE primary antibody (RAGE, sc-365154, Santa Cruz Biotechnology, Dallas, TX, USA). After washing with phosphate-buffered saline (PBS, Cytiva, Marlborough, MA, USA), the sections incubated with the anti-collagen type I primary antibody were treated with biotinylated secondary antibody goat anti-rabbit IgG (Vector Laboratories, Burlingame, CA, USA). The sections incubated with anti-collagen type II, anti-collagen type III, or anti-RAGE primary antibodies were treated with biotinylated secondary antibody anti-mouse IgG (Vector Laboratories, Burlingame, CA, USA). After washing with PBS, an avidin-biotin complex conjugated to peroxidase (Vector Laboratories, Burlingame, CA, USA) was utilized. The bound complexes were visualized by applying a DAB substrate (3,3'-diaminobenzidine, Vector Laboratories, Burlingame, CA, USA) to the sections. The images of the sections were taken by a light microscope (Leica, Wetzlar, Hesse, Germany). The average optical density (AOD) of all the IHC staining images were analyzed with the Immunohistochemistry Image Analysis Toolbox in ImageJ [38]. The H-DAB model was used for the IHC analysis, and the mean gray value was measured for semiquantification.

2.4. Second harmonic generation (SHG) imaging

The freshly isolated supraspinatus tendons with attached cartilage from newborn mice and the supraspinatus tendons with attached humerus bone from the other three groups were embedded in the super cryo-embedding medium (SCEM) (Section-lab, Hiroshima, Japan) without fixation or decalcification. Six tissue samples were utilized for the newborn mice group. Six tissue samples, with an equal number of males and females, were applied for the young, adult, and old groups. 20 μm thick sections were obtained by using cryostats (Leica CM1950, Wetzlar, Hesse, Germany) and were attached to the LCM film (Section-lab, Hiroshima, Japan). With the sectioned tissue sample facing upward, the LCM film was attached to a glass slide via transparent double-faced adhesive tape. The SHG imaging was performed by a SHG microscopy, as previously described [39]. In brief, the SHG microscopy consists of a mode-locked Ti:Sapphire fs laser (MaiTai DeepSee HP, SpectraPhysics, Milpitas, CA, USA) and a laser scanning microscope (BX61WI, Olympus, Center Valley, PA, USA). The fs laser system has a fixed wavelength of 800 nm, pulse duration of 100 fs, and repetition rate of 80 MHz. The laser power before entering the microscope was set to be 50 mW. For imaging, a long working distance objective lens (NA 0.45, 20×, Olympus, Center Valley, PA, USA) was used, and the excited SHG signals were filtered by a bandpass filter (Tavg > 93% 370 – 410 nm, Semrock, West Henrietta, NY) and then acquired by photomultiplier detectors. Stacks of 1024 × 1024-pixel images with a view field of 500 μm × 500 μm were obtained with a z step size of 300 nm. The collected SHG images were imported into FIJI software (National Institutes of Health, USA) for collagen fiber orientation analysis using the Directionality plugin, as previously described [40].

2.5 Collagen, GAG, and DNA contents

The supraspinatus tendon and attached cartilage in newborn mice were dissected closely to the insertion site. The supraspinatus tendon and attached humerus bone in the young, adult, and old groups were also isolated near the interfacial region. For the newborn group, five samples were put into an Eppendorf™ conical tube, and six tubes with 30 samples in total were utilized. For the young, adult, and old groups, one male and one female sample were put into Eppendorf™ conical tubes, and six tubes, for a total of 12 samples, were applied for each group. The samples were lyophilized, and the dry weights were measured. The tissue samples were homogenized by using a bead mill homogenizer (Fisher Scientific, Hampton, NH, USA) and further digested with 300 μg/ml papain in 50 mM phosphate buffer (pH 6.5), including 5 mM cysteine and 5 mM ethylenediamine tetraacetic acid (EDTA) for 16 h at 65 °C. The collagen content was determined with a hydroxyproline assay [41]. The samples were hydrolyzed using 4.8 N HCl. The dried hydrolysates were subsequently reacted with chloramine T reagent for oxidation. The Ehrlich's aldehyde reagent was added to the samples at 65 °C for 20 min to create chromospheres. The amount of hydroxyproline was measured via a microplate reader (Bio-Tek Instruments, Winooski, VT, USA) at 550 nm. A dimethylmethylene blue (DMMB) assay was utilized to quantify the sulfated GAG content [42]. A DMMB dye solution was added to the papain digested hydrolysates to promote the formation of the GAG-DMMB complex. The complex was then dissolved with a complex dissociation reagent containing guanidine hydrochloride, sodium acetate trihydrate, and 1-propanol. The amount of GAG was measured via the microplate reader at 656 nm. The DNA content was measured using a PicoGreen dsDNA quantification kit according to the manufacturer's instructions (Invitrogen, Waltham, MA, USA). Results for collagen, GAG, and DNA contents were normalized using the dry weight of the tissue samples and expressed in units of μg/mg.

2.6. Nanoindentation testing

The freshly isolated supraspinatus tendons with attached cartilage from newborn mice and supraspinatus tendons with attached humerus bones from the other three groups were prepared with the same approach mentioned in Section 2.4. Six tissue samples were utilized for each of the four groups. An equal number of males and females were used for the young, adult, and old groups. A 20 μm thick section was obtained by cryosection and attached to the LCM film, and the LCM film was attached to a glass slide with transparent double-faced adhesive tape. The section on the LCM film was rinsed with PBS and dried with absorbent paper before testing. A Triboindenter (Hysitron TI 950, EDEN Instruments, Alixan, France) was applied for the nanoindentation experiments. The probe used in the experiments was conical, and the diamond tip diameter was around 2 μm. The sectioned tissue sample was mounted on a glass slide without any glue. Displacement control was used, and a trapezoidal loading history was applied in three steps: 10 s loading, 5 s holding, and 10 s unloading. The loading and unloading rates were 200 nm/s. The force-displacement was obtained, and the associated reduced modulus was estimated directly from the machine. The reduced modulus E_r can be converted to Young's modulus E_s using the following equation:

$$\frac{1}{E_r} = \frac{1 - \upsilon_i^2}{E_i} + \frac{1 - \upsilon_s^2}{E_s}$$

where, the diamond tip, E_i, was 1140 GPa, and υ_i was 0.07. The Poisson's ratio of the specimen, υ_s, was assumed to be 0.3. The maximum load was also measured from the force-displacement results.

2.7. Uniaxial mechanical characterizations

Uniaxial testing was performed using a universal testing system (Test Resources, Shakopee, MN, USA) (Fig. 6A). A total of 30 mouse shoulder bone-rotator cuff complexes were subjected to the testing, i.e., 5 females and 5 males for each age group (excluding the newborn group, because the samples of the newborn group were too small and fragile for tensile testing). To achieve secure clamping without sample damage/slippage, a polymer tape was used to wrap and reinforce the attached muscular part to increase clamping friction and prevent clamping damage (Fig. 6B). The toothed clamp surfaces and the reinforcement wrapping worked well, and most of our uniaxial testing did not experience sample damage or slippage (22 successful tests out of 30). The mouse bone-rotator cuff complex was small in size and had a delicate muscular tissue, which caused certain challenges for sample preparation, mounting, and testing. We did experience one or two sample losses in each group due to damage/slippage. Before testing, the length, width, and thickness were measured at multiple locations using a Vernier digital caliper and averaged for dimension estimations. During the testing, samples were fully submerged in 1× PBS to create a physiological environment. After preconditioning, the sample was subjected to failure mechanical testing by being loaded at a ramping rate of 10 mm/s until it reached failure (Fig. 6C). Note that all uniaxial testing was started with a tare load of 0.5 g. Engineering stress was calculated by normalizing the applied force to the estimated original cross-sectional area, and engineering strain was calculated by normalizing the amount of sample deformation to the initial gauge length (the reference length of the tendon).

2.8. Isolation of tendon-to-bone interface tissues using LCM for proteomics processing

The freshly isolated supraspinatus tendon with attached cartilage from newborn mice and supraspinatus tendons with attached humerus bones in the young, adult, and old groups were embedded in a SCEM without fixation or decalcification [33]. Sections of 12 μm thickness were acquired with cryostats and attached to the LCM film. The LCM film was stuck to a plastic slide with a hole in it (Section-lab, Hiroshima, Japan). An LCM7000 (Leica, Wetzlar, Hesse, Germany) was used to isolate the tendon-to-bone interface tissue. The LCM parameters were listed as follows: power = 55, aperture = 12, speed = 15, specimen balance = 15, pulse frequency = 119, offset = 100. The micro-dissected enthesis samples were collected in a 0.2 ml thin-wall polymerase chain reaction (PCR) tube with a flat cup (Corning, Corning, NY, USA). The total collected area for each tube of the four groups was about 2.5-2.8 × 10^6 μm^2. For the newborn group, nine samples of the supraspinatus tendons with attached cartilage were cryo-sectioned and randomly micro-dissected into three PCR tubes. For the young, adult, and old groups, two male and two female samples of the

supraspinatus tendon with attached humerus bone were cryo-sectioned and then randomly micro-dissected into three PCR tubes for each group. The collected samples were lysed in 22 μL of cell lysis buffer, consisting of 5% sodium dodecyl sulfate (SDS) and 50mM triethylammonium bicarbonate (TEAB) at a pH of 7.55, and then sonicated (UP200St, Hielscher, Teltow, Germany) on ice for three 10-second intervals at 30% amplitude with 1-minute rest periods between intervals.

2.9. Suspension-Trapping (S-trap™) processing

An S-trap™ micro kit, including S-trap™ and included buffers (Protifi, Huntington, NY, USA), was used for sample processing. Briefly, each sample was reduced with 10 mM tris(2-carboxyethyl)phosphine in a thermomixer for 15 minutes set at 55°C at 1200 rpm, followed by alkylation with 20 mM methyl methanethiosulfonate in a thermomixer for 30 minutes at room temperature at 1200 rpm. 27.5% phosphoric acid was used to acidify the proteins, then samples were diluted with 165 μL of S-Trap™ binding buffer (100 mM TEAB, 90% methanol with pH 7.1). The samples were then loaded onto S-Trap™ micro spin columns and washed three times with S-Trap™ binding buffer. 20 μg of Trypsin-LysC in 50 mM TEAB in water solution was added to the top of the S-Trap™ and then incubated at 37°C for 2 hours. Peptides were eluted serially with 50 mM TEAB in water, 0.2% aqueous formic acid, and 50% acetonitrile containing 0.2% formic acid. Combined peptide elutions were vacuum centrifuged to dryness.

2.10. Mass spectrometry (MS)

Peptide samples were diluted to 0.2 μg/μL measured by a Pierce Quantitative Fluorometric Peptide Assay using a Varioskan LUX multimode microplate reader. The samples (5 μL; 1 μg per injection) were analyzed using a Dionex UltiMate™ 3000 RSLCnano liquid chromatography (LC) system coupled to an Orbitrap Exploris™ 480 mass spectrometer (Thermo Fisher Scientific, Waltham, MA, USA). Data acquisition and analysis settings are listed in supplementary information (Table S1&2). Data-dependent acquisition (DDA) and data-independent acquisition (DIA) sample sets, spiked with an iRT synthetic peptide mixture, were blocked and acquired in randomized order with digested *E. coli* injected immediately before and after every sixth sample to evaluate system performance. The consistency and reproducibility of the system performance were evaluated using QuiC (3.1.200602.47994).

2.11. MS Data analysis

DDA data were applied to create a spectral library using the Pulsar™ search engine in Spectronaut™ 14 (Biognosys, Switzerland). Default settings were used, with the exception that methylthio (C) was used as a fixed modification. Only precursors (*i.e.*, MSI of peptides) and proteins with a Qvalue of 0.01 were considered identified. Data were globally normalized to the median peptide signal. A minimum of 3 fragments was used for peptide quantification. Proteins with a P value<0.05 (Student's t test) and an absolute average log2 ratio >1 were considered differentially abundant between sample conditions. A volcano Plot was based on the results of the difference analysis (R version 3.6.1, ggplot2). The differential expression proteins (DEPs) were clustered and analyzed using the Hierarchical Cluster algorithm (pheatmap, 1.0.12).

2.12. Statistical analysis

One-way analysis of variance (ANOVA) and the Tukey *post hoc* test were applied for histological staining analysis, SHG imaging analysis, biochemical analysis, IHC analysis, and compressive testing analysis. The uniaxial mechanical testing was analyzed by two-way ANOVA. All statistical analyses were performed with GraphPad. Statistical significance is expressed as follows: *$p < 0.05$, **$p < 0.01$, ***$p < 0.001$.

3. Results

3.1. Collagen and proteoglycan distribution at the enthesis region

The H&E staining in Fig. 2A demonstrated the overall structure of the supraspinatus tendon-to-bone interface in the four groups. The histological framework of the newborn group had a higher cell density and less organized cell or fiber orientation, which showed distinct differences from the other three groups. The similarities of the histological structures for the young, adult, and old groups were observed. Masson's Trichrome staining illustrated the collagen distribution at the interface region in a blue color. The proportion of the collagen's area was significantly decreased in the young, adult, and old groups compared with the newborn group (Fig. 2B). The red color in the Safranin O staining represented the proteoglycan deposition at the enthesis region. The proportion of the proteoglycan deposition area, or the metachromasia area, was lower in the young group than in the newborn group. The proportion of the proteoglycan deposition area then increased in the old group compared to the young and adult groups (Fig. 2C). The orange and green colors in the PR staining exhibited the thick and thin collagen fibers, respectively. The ratio of the thin fibers to thick fibers increased with age (Fig. 2D). No significant differences of the histological staining were observed between the males and females within the young, adult, or old group.

3.2. Collagen fiber organization at the enthesis region

Fig. 3A shows the SHG images of the supraspinatus tendon-to-bone interface in the newborn, young, adult, and old groups. Fig. 3B displays the representative dispersion graph of the collagen fibers at the enthesis area of each group. The dispersion of collagen fibers was significantly decreased in the young and adult groups compared to the newborn group (young: $13.74 \pm 5.24°$; adult: $14.68 \pm 5.73°$; old: $23.41 \pm 4.58°$), indicating more organized collagen fibers in the young and adult groups. The collagen fiber orientation became less organized in the old group, with the dispersion increasing to $19.47 \pm 5.34°$, but the differences among the young, adult, and old groups were not significant (Fig. 3C). No significant differences of the collagen fiber organization were observed between the males and females within the young, adult, or old group.

3.3. Collagen, GAG, and DNA contents

The supraspinatus tendon with attached humerus cartilage or bone units were isolated closely to the supraspinatus enthesis region for all four age groups. The harvested tissues were disrupted to measure the collagen, GAG, and DNA contents. The collagen content in the newborn group was significantly higher than that in the young, adult, and old groups

(newborn: 55.26 ± 6.91 μg/mg; young: 21.57 ± 3.08 μg/mg; adult: 25.62 ± 4.52 μg/mg; old: 24.82 ± 3.44 μg/mg) (Fig. 3D). The GAG content significantly decreased in the young, adult, and old groups compared with the newborn group (newborn: 13.53 ± 2.30 μg/mg; young: 4.06 ± 0.53 μg/mg; adult: 4.86 ± 0.62 μg/mg; old: 4.60 ± 1.06 μg/mg) (Fig. 3E). The DNA content was also significantly higher in the newborn group compared to the young, adult, and old groups (newborn: 4.37 ± 1.47 μg/mg; young: 1.37 ± 0.33 μg/mg; adult: 1.56 ± 0.41 μg/mg; old: 1.06 ± 0.34 μg/mg) (Fig. 3F), indicating changes in cell numbers.

3.4. Types I, II, and III collagen and RAGE distribution

Fig. 4A demonstrates the distribution of types I, II, and III collagen and RAGE in the four age groups. The highest type I collagen stain intensity was observed at the supraspinatus tendon region. Some type I collagen was also observed in the cartilage/bone region in the newborn group. Type II collagen was mainly located at the tendon-to-bone interface region. Type III collagen was lightly stained, and the highest stain intensity was at the supraspinatus tendon region. RAGE was also concentrated in the supraspinatus tendon region. The average optical density (AOD) of the type I collagen was significantly higher in the newborn group than in the adult and old groups (Fig. 4B). The AOD of types II and III collagen and RAGE did not show distinct differences (Fig. 4C-E). No significant differences of the distribution and AOD of the type I, II, and III collagens and RAGE were observed between the males and females within the young, adult, or old group.

3.5. Nanoindentation testing of the enthesis regions

Nanoindentation has been used to test the mechanical property changes across soft-to-hard tissue interfaces [43]. It can provide specifically localized mechanical assessment of heterogeneous biomaterials with high resolution [44]. We applied the nanoindentation tip to two enthesis regions, i.e., one region close to tendon and one region close to bone (for young, adult, and old groups)/cartilage (for newborn group) (Fig. 5A & D). The representative load-depth curve for each group is illustrated in Fig. 5G. The maximum load of the enthesis at the site near the tendon increased with maturation, peaked at adult stage, and dropped at old stage (not significant) (newborn: 532.34 ± 139.98 μN; young: 826.99 ± 544.92 μN; adult: 1383.55 ± 572.67 μN; old: 869.45 ± 413.18 μN) (Fig. 5B). The Young's modulus of the enthesis at the site near the tendon demonstrated a similar trend, i.e., increased with maturation, peaked at adult stage, and silghtly dropped at old stage (newborn: 0.098 ± 0.023 GPa; young: 0.16 ± 0.11 GPa; adult: 0.28 ± 0.12 GPa; old: 0.23 ± 0.13 GPa) (Fig. 5C). The maximum load of the enthesis near the bone/cartilage also showed similar trend (newborn: 572.73 ± 57.51 μN; young: 1161.32 ± 400.59 μN; adult: 1402.14 ± 221.20 μN; old: 927.38 ± 256.26 μN) (Fig. 5E). The Young's modulus of the enthesis near the bone/cartilage again showed a similar trend, but the difference between the adult and old groups was not significant (newborn: 0.105 ± 0.009 GPa; young: 0.34 ± 0.18 GPa; adult: 0.36 ± 0.10 GPa; old: 0.25 ± 0.10 GPa) (Fig. 5F). No significant differences of the maximum load and Young's modulus for both indentation sites were observed between the males and females within the young, adult, or old group.

3.6. Uniaxial mechanical behaviors and failure properties

The failure stress-strain curves of the bone-rotator cuff complex were plotted in Fig. 6D. The failure stress, failure strain, and maximum tensile modulus were obtained from the stress-strain curves. For the maximum tensile modulus, a short curve section before the yielding point was used for linear fitting to calculate the modulus value. The overall trends among young, adult, and old groups, as well as female versus male, are demonstrated in Fig. 6E-G. For failure stress (mechanical strength), no difference between young and adult mice was found, while old mice showed increased failure stress, especially the old male mice (young female: 662.83 ± 115.14 kPa; young male: 673.34 ± 167.22 kPa; adult female: 468.59 ± 67.52 kPa; adult male: 668.74 ± 184.74 kPa; old female: 899.05 ± 467.39 kPa; old male: 1548.50 ± 153.68 kPa). The maximum tensile modulus represents the stiffness of the complex. An increasing trend was observed from young, to adult, to old mice, but only the difference between old male and young female groups was significant (young female: 7.41 ± 4.04 MPa; young male: 22.95 ± 11.16 MPa; adult female: 16.75 ± 6.83 MPa; adult male: 24.76 ± 9.05 MPa; old female: 16.80 ± 3.68 MPa; old male: 32.71 ± 9.13 MPa). No obvious trend exists in the failure strain, except the complexes of young females had larger failure strains (more extensible) compared with the young male and adult male groups (young female: 0.11 ± 0.03%; young male: 0.036 ± 0.011%; adult female: 0.042 ± 0.015%; adult male: 0.040 ± 0.004%; old female: 0.073 ± 0.034%; old male: 0.074 ± 0.031%). Lastly, the male mice had higher overall failure stresses than the female mice in adult and old groups (Fig. 6E), and the male mice had larger overall maximum tensile moduli than the female mice in all three age groups (Fig. 6G). However, the differences between male and female mice in each group were not significant.

3.7. Proteomics sample preparation and analysis

The sample preparation process for LC-MS and proteomics analysis is shown in Fig. 7A. SCEM was applied to embed the freshly isolated tendon-cartilage units from the newborn group or tendon-bone units from the young, adult, and old groups without fixation and decalcification. The cryo-sectioned tendon-cartilage or tendon-bone unit was mounted on an LCM film, and the LCM film was attached to a plastic slide with a hole in it. The tendon-to-cartilage interface was isolated using an LCM machine for the newborn group (Fig. 7B & C). The tendon-to-bone interfaces were also harvested for the young, adult, and old groups (Fig. 7D & E). The isolated entheses were collected in the caps of PCR tubes with lysis buffer in them (Fig. 7F). An S-trap kit was used for the proteomics sample preparation. Mass spectrometry and data analysis were then performed.

In total, 968 proteins were identified for all the four groups. The protein profile in the newborn group was strikingly distinguished from the other three groups, and the protein profiles in the young, adult, and old groups were similar (Fig. 8A). The four age groups shared 813 proteins in common, while 33 proteins were only observed in the newborn group, and no unique protein was observed in the other three groups (Fig. 8B). The volcano plot of the young and newborn groups revealed dramatic protein abundance changes, with 141 lower abundance proteins and 123 higher abundance proteins in the young group compared to the newborn group (Fig. 8C). The top 20 low abundance proteins and top 20 higher abundance proteins are listed in Fig. 8C. The Gene Ontology (GO) analysis

and the Kyoto Encyclopedia of Genes and Genomes (KEGG) pathway annotation were performed. The differentially abundant proteins were primarily from cells and extracellular regions and participated in binding, catalytic activity, and structural molecule activity for the molecular functions (Fig. S1A). The KEGG pathway annotation demonstrated the differentially abundant proteins were mainly involved in ECM-receptor interaction, focal adhesion, carbon metabolism, the protein processing endoplasmic reticulum, and the PI3K-Akt signaling pathway (Fig. S1B). The protein-protein interaction network is shown in Fig. S2. For the comparison of adult and young groups, only 2 proteins were lower abundance and 11 proteins were higher abundance in the adult group compared to the young group (Fig. S3). The protein profile of the old and adult groups was also similar. There were 28 lower abundance proteins and 15 higher abundance proteins in the old group compared to the adult group. The top 20 lower abundance proteins and 13 higher abundance proteins, with their names, are listed in Fig. 8D. The GO analysis and KEGG pathway annotation are illustrated in Fig. S4A & B.

4. Discussion

In this study, we have systematically characterized the molecular, histological, and biomechanical changes at the rotator cuff tendon-to-bone interface in four different age groups. In general, distinguished differences were observed between the newborn and young group (maturation process), while there were not many differences among the young, adult, and old groups (aging process).

The histological results indicated a decreased proteoglycan content and more organized collagen fibers at the interface area during the maturation process, which were also found in a previous study [25]. Because of the inclusion of an old age group in the study, an increasing proteoglycan content and less organized collagen fibers were also identified during the aging process by comparing the differences between adult and old age groups. Masson's Trichrome staining and quantitative collagen content measurement showed decreased collagen distribution at the interfacial region during the maturation process. The decreasing cellularity at the interface region during the maturation process was shown in the H&E staining and confirmed with DNA content measurement. There was not much alteration of type II collagen distribution among the four age groups, which was also found in the previous study [25]. The accumulation of AGE has been correlated with the progression of many diseases related to aging [45]. However, no distinct differences of RAGE distributions were found at the tendon-to-bone interfaces among the four age groups in our study. IHC can only evaluate the distribution and accumulation of AGE at the two-dimensional level without precisely quantitative measurement [46]. The immunological detection method also has the problem of non-specific binding of the antibody [47]. Thus, other high accuracy quantitative studies of AGE are needed. With the improvements in instrumentation, mass spectrometry might be a promising strategy for the targeted AGE measurement [48].

Age-dependent alterations of the local tissue compressive mechanical properties and the tensile mechanical properties of the humerus bone-supraspinatus tendon complex were characterized in this study. Nanoindentation testing showed that the maximum load and Young's modulus at the enthesis increased during the maturation process, peaked at adult

stage, and slightly decreased at old stage. The measured modulus value correlated with the mineral content in the tested sample [49]. An increased modulus indicated an elevated mineralization level in the tissue sample. ALP is an enzyme that is highly expressed in cell-mediated mineralization [50]. Our proteomics data showed that the ALP protein level was more abundant in the young group compared to the newborn group and lower abundant in the old group compared to the adult group. This may partially explain the trend of compressive mechanical property alterations with maturation and aging. The limitation of indentation testing is the control of hydration status. With the alteration of the hydration status, mechanical properties for the tendon region in the tendon-bone complex's sections varied. To keep the moisture level consistent among each group, the sectioned samples were moistened before testing with the same amount of PBS droplets for the same period of time [51]. Thus, the nanoindentation results might not precisely represent the properties of the enthesis under physiological conditions. Otherwise, the trend among the four age groups should indicate the alteration of mechanical properties with age.

The results of uniaxial tensile mechanical testing on humerus bone-supraspinatus tendon complex showed some interesting observation. The failure stress in the old group, especially the old male group, increased significantly compared to the young and adult groups. The maximum tensile modulus also showed an increasing trend from the young to old groups, but the difference was only significant between the old male group and the young female group. The increased area of fibrocartilage in the Safranin O staining at the enthesis insertion site might explain the increased complex stiffness and failure stress at the old group. The fibrocartilage zone plays an essential role in the mechanical-loading transition between the tendon and bone tissues. A lack of fibrocartilage formation after rotator cuff injury repair usually results in a retear or recurrence at the enthesis [52]. The accumulation of fibrocartilage might lead to augmented enthesis strength. Since the failure stress of the enthesis increased with age in this study, it contradicted our expectation and hypothesis. Therefore, for the mouse model, age alone might not be the dominant risk factor for increased rotator cuff injury rate. Other factors associated with the aging process, like overuse, accumulated tissue damages/injuries, and underlying chronic disease, might contribute to the vulnerability of the rotator cuff in the elderly populations [53, 54].

We combined LCM and Kawamot's film methods to isolate the tendon-to-bone interface without fixation and decalcification. Due to the unclear boundary of the interface with tendon and bone, a small amount of tendon or bone tissues were collected together with the interface tissues. The collected tissues were then applied for proteomics analysis. Some proteins were found to play essential roles in the enthesis during the maturation and aging processes. Among the lower abundance proteins in the young group compared with the newborn group, we detected non-collagenous ECM proteins, matrilin-1, and matrilin-4, which were primarily expressed in cartilage and participated in the modulation of ECM assembly [55, 56]. We also detected three types of collagens: collagen type XIV (alpha-1), collagen type IX (alpha-1), and collagen type XI (alpha-2). Collagen type IX and collagen type XIV are categorized as the collagen subfamily of fibril-associated collagens with interrupted triple helices (FACIT), and collagen type XI belongs to the fibrillar collagens [57]. Collagen type XI controls collagen fibrillogenesis and is associated with both tendon and cartilage collagen fibril assembly and organization [58, 59]. FACIT collagens adhere to

the exterior of the microfibril and interact with small leucine-rich repeat proteoglycans (SLRP) to result in a higher-order structure [57]. Chondroadherin belongs to the SLRP [60] and was also found in the downregulated proteins in the young age group. Among the higher abundance proteins in the young group compared with the newborn group, we found ALP, fibrillin-1, and Cu-Zn superoxide dismutase (SOD1). ALP is associated with cell-mediated mineralization [50], indicating increased mineralization at the tendon-to-bone interface during the maturation process. Fibrillin is a non-collagenous ECM protein that forms the structure of microfibrils, contributing to the elasticity of the connective tissue [61]. SOD1 is an enzyme that scavenges superoxide anions, and elevated SOD1 might relate to the adaptation of the postnatal environment [62]. As for the lower abundance proteins in the old group compared with the adult group, we detected matrix metalloproteinase-9 (MMP9), collagen type XI, and ALP. MMP9 can degrade the components of the ECM and participate in the growth and development of cartilage and bone tissues [63]. The lower abundance of collagen type XI might indicate compositional changes of the collagen fibrils with age. The reduced ALP levels might suggest decreased mineralization levels at the tendon-to-bone interface with age. Elastin is upregulated in the old group compared to the adult group. Elastin is a non-collagenous ECM protein essential to the elasticity and resilience of connective tissues, like tendon and cartilage [64]. The increase of elastin may also contribute to the increase of the failure stress in the old group.

We systematically characterized the variations of the rotator cuff tendon-to-bone interface during the maturation process (from newborn to young or adult). For histological changes at the enthesis, we found decreased proteoglycan and collagen deposition, reduced cellularity, increased thin collagen fiber ratio, and a more organized collagen fiber orientation. For biomechanical analysis, the maximum load and Young's modulus of the nanoindentation testing were increased, while the uniaxial tensile testing did not show significant changes. For proteomics analysis, dramatic alterations of protein profiles from newborn to young were detected. We also evaluated the variations of the rotator cuff tendon-to-bone interface during the aging process (from adult to old). For the histology, proteoglycan deposition increased at the enthesis, and the collagen fiber orientation demonstrated a trend of being less organized with aging. For biomechanical testing, the maximum load and Young's modulus of the nanoindentation testing showed a decreasing trend, while the uniaxial tensile testing revealed a significant increase of failure stress with aging, especially for the old male group. The protein profiles of the adult and old age groups showed similarities, and several proteins were identified that might play critical roles during the aging process of the rotator cuff tendon-to-bone interface.

In summary, our observations demonstrated the histological, biomechanical, and molecular alterations of the rotator cuff tendon-to-bone interface with age. Major molecular, histological, and mechanical changes primarily occur during the maturation process. A large animal model or human tissue samples for aging studies of the tendon-to-bone interface is needed to confirm the findings of this study. Detailed investigations with gene-deficient or knockout models are necessary to elucidate the function of these molecular changes during maturation and aging that we detected in the proteomics study. Based on the uniaxial tensile mechanical testing result, aging might not be the dominant risk factor for the increased prevalence of enthesis diseases. Other potential risk factors of rotator cuff injuries associated

with the aging process, like overuse, chronic injuries, and hormone level, should be studied during the aging process. These studies will inspire new methods to prevent the onset of the enthesis diseases and encourage novel strategies for the rotator cuff enthesis regeneration by recapitulating the structural, mechanical, and compositional properties of the mature enthesis.

Supplementary Material

Refer to Web version on PubMed Central for supplementary material.

Acknowledgements

This work is supported by National Institute of Health (NIH R01 AR073225) for B.D and P.S and supported by University of Nebraska Collaboration Initiative Seed Grant for B.D. and M.F. X.J is partially supported by the China Scholarship Council and UNMC fellowship. The author would like to thank the Tissue Science Core Facility of UNMC for the assistance with histological staining and Dr. Wenlong Li from University of Nebraska-Lincoln for the aid with the nanoindentation testing.

Abbreviations

ACL	Anterior cruciate ligament
AGE	Advanced glycation end
ALP	Alkaline phosphatase
ANOVA	Analysis of variance
AOD	Average optical density
DDA	Data-dependent acquisition
DEP	Differential expression protein
DIA	Data-independent acquisition
DMMB	Dimethylmethylene blue
ECM	Extracellular matrices
EDTA	Ethylenediamine tetraacetic acid
FACIT	Fibril-associated collagens with interrupted triple helices
FDR	False discovery rate
GAG	Glycosaminoglycan
GO	Gene ontology
H&E	Hematoxylin and eosin
IHC	Immunohistochemistry
KEGG	Kyoto encyclopedia of genes and genomes

LC	Liquid chromatography
LCM	Laser captured microdissection
MMP9	Matrix metalloproteinase-9
MS	Mass spectrometry
MT	Masson’s trichrome
PBS	Phosphate buffered saline
PCR	Polymerase chain reaction
PR	Picrosirius red
RAGE	Receptor for advanced glycation end product
SCEM	Super Cryo-embedding Medium
SDS	Sodium dodecyl sulfate
SHG	Second harmonic generation
SLRP	Small leucine-rich repeat proteoglycans
SO	Safranin O
SOD1	Cu-Zn superoxide dismutase
TEAB	Triethylammonium bicarbonate

Reference

1. Yamaguchi K, Ditsios K, Middleton WD, Hildebolt CF, Galatz LM, and Teefey SA (2006) The demographic and morphological features of rotator cuff disease. A comparison of asymptomatic and symptomatic shoulders. J Bone Joint Surg Am 88, 1699–1704 [PubMed: 16882890]
2. Oh LS, Wolf BR, Hall MP, Levy BA, and Marx RG (2007) Indications for rotator cuff repair: a systematic review. Clin Orthop Relat Res 455, 52–63 [PubMed: 17179786]
3. van der Windt DA, Koes BW, de Jong BA, and Bouter LM (1995) Shoulder disorders in general practice: incidence, patient characteristics, and management. Ann Rheum Dis 54, 959–964 [PubMed: 8546527]
4. Milgrom C, Schaffler M, Gilbert S, and van Holsbeeck M (1995) Rotator-cuff changes in asymptomatic adults. The effect of age, hand dominance and gender. J Bone Joint Surg Br 77, 296–298 [PubMed: 7706351]
5. Teunis T, Lubberts B, Reilly BT, and Ring D (2014) A systematic review and pooled analysis of the prevalence of rotator cuff disease with increasing age. J Shoulder Elbow Surg 23, 1913–1921 [PubMed: 25441568]
6. Diebold G, Lam P, Walton J, and Murrell GA (2017) Relationship between age and rotator cuff retear: a study of 1,600 consecutive rotator cuff repairs. J Bone Joint Surg Am 99, 1198–1205 [PubMed: 28719559]
7. Lee YS, Jeong JY, Park CD, Kang SG, and Yoo JC (2017) Evaluation of the Risk Factors for a Rotator Cuff Retear After Repair Surgery. Am J Sports Med 45, 1755–1761 [PubMed: 28319431]
8. Saveh-Shemshaki N, N SL, and Laurencin CT (2019) Nanofiber-based matrices for rotator cuff regenerative engineering. Acta Biomater 94, 64–81 [PubMed: 31128319]

9. Apostolakos J, Durant TJ, Dwyer CR, Russell RP, Weinreb JH, Alaee F, Beitzel K, McCarthy MB, Cote MP, and Mazzocca AD (2014) The enthesis: a review of the tendon-to-bone insertion. Muscles Ligaments Tendons J 4, 333–342 [PubMed: 25489552]
10. Smith L, Xia Y, Galatz LM, Genin GM, and Thomopoulos S (2012) Tissue-engineering strategies for the tendon/ligament-to-bone insertion. Connect Tissue Res 53, 95–105 [PubMed: 22185608]
11. Lui P, Zhang P, Chan K, and Qin L (2010) Biology and augmentation of tendon-bone insertion repair. J Orthop Surg Res 5, 59 [PubMed: 20727196]
12. Lu HH, and Thomopoulos S (2013) Functional Attachment of Soft Tissues to Bone: Development, Healing, and Tissue Engineering. Annu Rev Biomed Eng 15, 201–226 [PubMed: 23642244]
13. Benjamin M, Kumai T, Milz S, Boszczyk BM, Boszczyk AA, and Ralphs JR (2002) The skeletal attachment of tendons—tendon 'entheses'. Comp Biochem Physiol A Mol Integr Physiol 133, 931–945 [PubMed: 12485684]
14. Gulotta LV, and Rodeo SA (2009) Growth Factors for Rotator Cuff Repair. Clin Sports Med 28, 13–23 [PubMed: 19064162]
15. Tellado SF, Balmayor ER, and Van Griensven M (2015) Strategies to engineer tendon/ligament-to-bone interface: Biomaterials, cells and growth factors. Adv Drug Deliv Rev 94, 126–140 [PubMed: 25777059]
16. Saito M, and Marumo K (2010) Collagen cross-links as a determinant of bone quality: a possible explanation for bone fragility in aging, osteoporosis, and diabetes mellitus. Osteoporos Int 21, 195–214 [PubMed: 19760059]
17. Li Y, Fessel G, Georgiadis M, and Snedeker JG (2013) Advanced glycation end-products diminish tendon collagen fiber sliding. Matrix Biol 32, 169–177 [PubMed: 23348249]
18. Odetti P, Rossi S, Monacelli F, Poggi A, Cirnigliaro M, Federici M, and Federici A (2005) Advanced glycation end products and bone loss during aging. Ann N Y Acad Sci 1043, 710–717 [PubMed: 16037297]
19. Blitz E, Sharir A, Akiyama H, and Zelzer E (2013) Tendon-bone attachment unit is formed modularly by a distinct pool of Scx-and Sox9-positive progenitors. Development 140, 2680–2690 [PubMed: 23720048]
20. Sugimoto Y, Takimoto A, Akiyama H, Kist R, Scherer G, Nakamura T, Hiraki Y, and Shukunami C (2013) Scx+/Sox9+ progenitors contribute to the establishment of the junction between cartilage and tendon/ligament. Development 140, 2280–2288 [PubMed: 23615282]
21. Thomopoulos S, Kim HM, Rothermich SY, Biederstadt C, Das R, and Galatz LM (2007) Decreased muscle loading delays maturation of the tendon enthesis during postnatal development. J Orthop Res 25, 1154–1163 [PubMed: 17506506]
22. Thomopoulos S, Kim HM, Silva MJ, Ntouvali E, Manning CN, Potter R, Seeherman H, and Gelberman RH (2012) Effect of bone morphogenetic protein 2 on tendon-to-bone healing in a canine flexor tendon model. J Orthop Res 30, 1702–1709 [PubMed: 22618762]
23. Schwartz A, Lipner J, Pasteris J, Genin G, and Thomopoulos S (2013) Muscle loading is necessary for the formation of a functional tendon enthesis. Bone 55, 44–51 [PubMed: 23542869]
24. Plate JF, Brown PJ, Walters J, Clark JA, Smith TL, Freehill MT, Tuohy CJ, Stitzel JD, and Mannava S (2014) Advanced age diminishes tendon-to-bone healing in a rat model of rotator cuff repair. Am J Sports Med 42, 859–868 [PubMed: 24500915]
25. Wang INE, Mitroo S, Chen FH, Lu HH, and Doty SB (2006) Age-dependent changes in matrix composition and organization at the ligament-to-bone insertion. J Orthop Res 24, 1745–1755 [PubMed: 16779829]
26. Tanaka E, Tanaka M, Hattori Y, Aoyama J, Watanabe M, Sasaki A, Sugiyama M, and Tanne K (2001) Biomechanical behaviour of bovine temporomandibular articular discs with age. Arch Oral Biol 46, 997–1003 [PubMed: 11543706]
27. Tuma H, Venable J, Wuthier P, and Henrickson R (1962) Relationship of fiber diameter to tenderness and meatiness as influenced by bovine age. J Anim Sci 21, 33–36
28. Zhang H, Lin S, Chen X, Gu L, Zhu X, Zhang Y, Reyes K, Wang B, and Jin K (2019) The effect of age, sex and strains on the performance and outcome in animal models of stroke. Neurochem Int 127, 2–11 [PubMed: 30291954]

29. Emmert-Buck MR, Bonner RF, Smith PD, Chuaqui RF, Zhuang Z, Goldstein SR, Weiss RA, and Liotta LA (1996) Laser capture microdissection. Science 274, 998–1001 [PubMed: 8875945]
30. Espina V, Wulfkuhle JD, Calvert VS, VanMeter A, Zhou W, Coukos G, Geho DH, Petricoin EF, and Liotta LA (2006) Laser-capture microdissection. Nat Protoc 1, 586–603 [PubMed: 17406286]
31. Killian ML, and Thomopoulos S (2016) Scleraxis is required for the development of a functional tendon enthesis. FASEB J 30, 301–311 [PubMed: 26443819]
32. Schwartz AG, Long F, and Thomopoulos S (2015) Enthesis fibrocartilage cells originate from a population of Hedgehog-responsive cells modulated by the loading environment. Development 142, 196–206 [PubMed: 25516975]
33. Kawamoto T, and Kawamoto K (2014) Preparation of thin frozen sections from nonfixed and undecalcified hard tissues using Kawamot's film method (2012). In Methods Mol Biol pp. 149–164, Springer
34. Van De Vlekkert D, Machado E, and d'Azzo A (2020) Analysis of Generalized Fibrosis in Mouse Tissue Sections with Masson's Trichrome Staining. Bio Protoc 10, e3629–e3629
35. Degen RM, Carbone A, Carballo C, Zong J, Chen T, Lebaschi A, Ying L, Deng X-H, and Rodeo SA (2016) The Effect of Purified Human Bone Marrow–Derived Mesenchymal Stem Cells on Rotator Cuff Tendon Healing in an Athymic Rat. Arthroscopy 32, 2435–2443 [PubMed: 27282111]
36. Zerbinati N, and Calligaro A (2018) Calcium hydroxylapatite treatment of human skin: evidence of collagen turnover through picrosirius red staining and circularly polarized microscopy. Clin Cosmet Investig Dermatol 11, 29–35
37. Rich L, and Whittaker P (2017) Collagen and picrosirius red staining: a polarized light assessment of fibrillar hue and spatial distribution. J Morphol Sci 22, 0–0
38. Shu J, Qiu G, and Mohammad I (2013) A Semi-automatic Image Analysis Tool for Biomarker Detection in Immunohistochemistry Analysis. In 2013 Seventh International Conference on Image and Graphics pp. 937–942
39. Li D, Huang X, Xiao Z, Chen H, Zhang L, Hao Y, Song J, Shao D-F, Tsymbal EY, and Lu Y (2020) Polar coupling enabled nonlinear optical filtering at MoS 2/ferroelectric heterointerfaces. Nat Commun 11, 1–8 [PubMed: 31911652]
40. Bah I, Fernandes NR, Chimenti RL, Ketz J, Flemister AS, and Buckley MR (2020) Tensile mechanical changes in the Achilles tendon due to Insertional Achilles tendinopathy. J Mech Behav Biomed Mater 112, 104031 [PubMed: 32882677]
41. Duan B, Yin Z, Hockaday Kang L, Magin RL, and Butcher JT (2016) Active tissue stiffness modulation controls valve interstitial cell phenotype and osteogenic potential in 3D culture. Acta Biomater 36, 42–54 [PubMed: 26947381]
42. Duan B, Hockaday LA, Das S, Xu C, and Butcher JT (2015) Comparison of mesenchymal stem cell source differentiation toward human pediatric aortic valve interstitial cells within 3D engineered matrices. Tissue Eng Part C Methods 21, 795–807 [PubMed: 25594437]
43. Armitage OE, and Oyen ML (2017) Indentation across interfaces between stiff and compliant tissues. Acta Biomater 56, 36–43 [PubMed: 28062353]
44. Abraham AC, and Donahue TL (2013) From meniscus to bone: a quantitative evaluation of structure and function of the human meniscal attachments. Acta Biomater 9, 6322–6329 [PubMed: 23385217]
45. Chaudhuri J, Bains Y, Guha S, Kahn A, Hall D, Bose N, Gugliucci A, and Kapahi P (2018) The Role of Advanced Glycation End Products in Aging and Metabolic Diseases: Bridging Association and Causality. Cell Metab 28, 337–352 [PubMed: 30184484]
46. Suzuki A, Yabu A, and Nakamura H (2020) Advanced glycation end products in musculoskeletal system and disorders. Methods
47. Thornalley PJ (2005) Measurement of Protein Glycation, Glycated Peptides, and Glycation Free Adducts. Perit Dial Int 25, 522–533 [PubMed: 16419322]
48. Soboleva A, Vikhnina M, Grishina T, and Frolov A (2017) Probing Protein Glycation by Chromatography and Mass Spectrometry: Analysis of Glycation Adducts. Int J Mol Sci 18

49. Hauch K, Oyen M, Odegard G, and Donahue TH (2009) Nanoindentation of the insertional zones of human meniscal attachments into underlying bone. J Mech Behav Biomed Mater 2, 339–347 [PubMed: 19627840]
50. Golub EE, and Boesze-Battaglia K (2007) The role of alkaline phosphatase in mineralization. Curr Opin Orthop 18, 444–448
51. Aifantis KE, Shrivastava S, and Odegard GM (2011) Transverse mechanical properties of collagen fibers from nanoindentation. J Mater Sci Mater Med 22, 1375–1381 [PubMed: 21556981]
52. Zhou Y, Zhang J, Yang J, Narava M, Zhao G, Yuan T, Wu H, Zheng N, Hogan MV, and Wang JHC (2017) Kartogenin with PRP promotes the formation of fibrocartilage zone in the tendon–bone interface. J Tissue Eng Regen Med 11, 3445–3456 [PubMed: 28127950]
53. Abate M, Schiavone C, Di Carlo L, and Salini V (2014) Prevalence of and risk factors for asymptomatic rotator cuff tears in postmenopausal women. Menopause 21, 275–280 [PubMed: 23760436]
54. Abate M, Di Carlo L, Salini V, and Schiavone C (2017) Risk factors associated to bilateral rotator cuff tears. Orthop Traumatol Surg Res 103, 841–845 [PubMed: 28578100]
55. Deák F, Wagener R, Kiss I, and Paulsson M (1999) The matrilins: a novel family of oligomeric extracellular matrix proteins. Matrix Biol 18, 55–64 [PubMed: 10367731]
56. Klatt AR, Becker AK, Neacsu CD, Paulsson M, and Wagener R (2011) The matrilins: modulators of extracellular matrix assembly. Int J Biochem Cell Biol 43, 320–330 [PubMed: 21163365]
57. Mouw JK, Ou G, and Weaver VM (2014) Extracellular matrix assembly: a multiscale deconstruction. Nat Rev Mol Cell Biol 15, 771–785 [PubMed: 25370693]
58. Mendler M, Eich-Bender SG, Vaughan L, Winterhalter KH, and Bruckner P (1989) Cartilage contains mixed fibrils of collagen types II, IX, and XI. J Cell Biol 108, 191–197 [PubMed: 2463256]
59. Sun M, Luo EY, Adams SM, Adams T, Ye Y, Shetye SS, Soslowsky LJ, and Birk DE (2020) Collagen XI regulates the acquisition of collagen fibril structure, organization and functional properties in tendon. Matrix Biol 94, 77–94 [PubMed: 32950601]
60. Paracuellos P, Kalamajski S, Bonna A, Bihan D, Farndale RW, and Hohenester E (2017) Structural and functional analysis of two small leucine-rich repeat proteoglycans, fibromodulin and chondroadherin. Matrix Biol 63, 106–116 [PubMed: 28215822]
61. Kielty CM, Baldock C, Lee D, Rock MJ, Ashworth JL, and Shuttleworth CA (2002) Fibrillin: from microfibril assembly to biomechanical function. Philos Trans R Soc Lond B Biol Sci 357, 207–217 [PubMed: 11911778]
62. Zelko IN, Mariani TJ, and Folz RJ (2002) Superoxide dismutase multigene family: a comparison of the CuZn-SOD (SOD1), Mn-SOD (SOD2), and EC-SOD (SOD3) gene structures, evolution, and expression. Free Radic Biol Med 33, 337–349 [PubMed: 12126755]
63. Vandooren J, Van den Steen PE, and Opdenakker G (2013) Biochemistry and molecular biology of gelatinase B or matrix metalloproteinase-9 (MMP-9): the next decade. Crit Rev Biochem Mol Biol 48, 222–272 [PubMed: 23547785]
64. Mithieux SM, and Weiss AS (2005) Elastin. Adv Protein Chemistry 70, 437–461

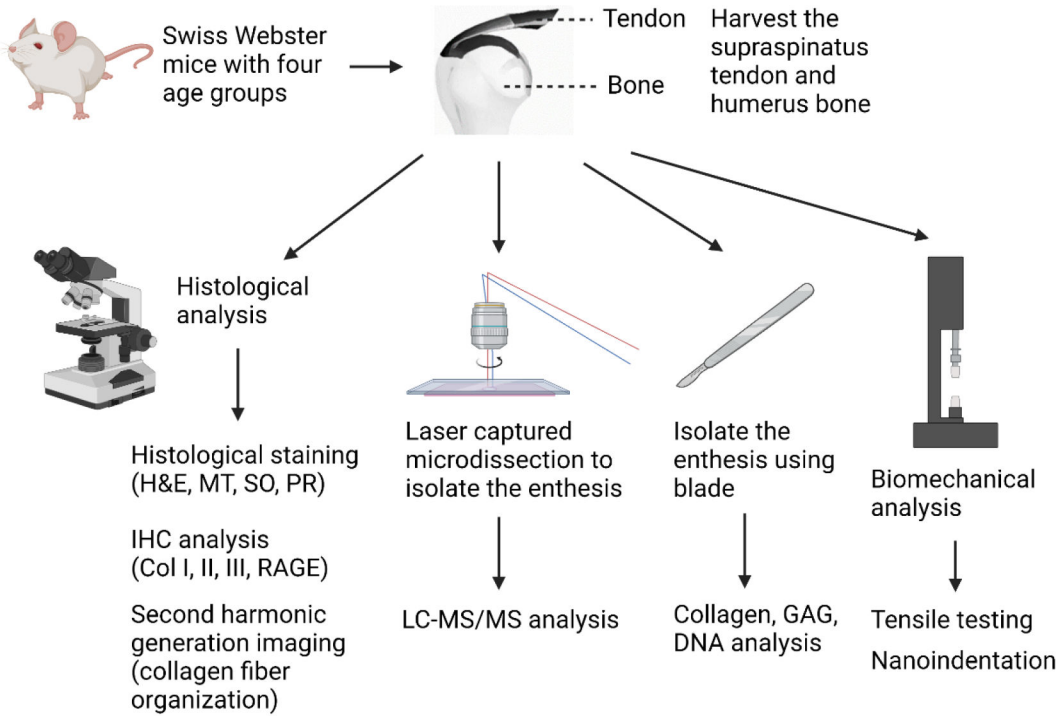

Figure 1.

Schematics of study design to identify the effects of maturation and aging on the rotator cuff tendon-to-bone interface. Created with BioRender.com.

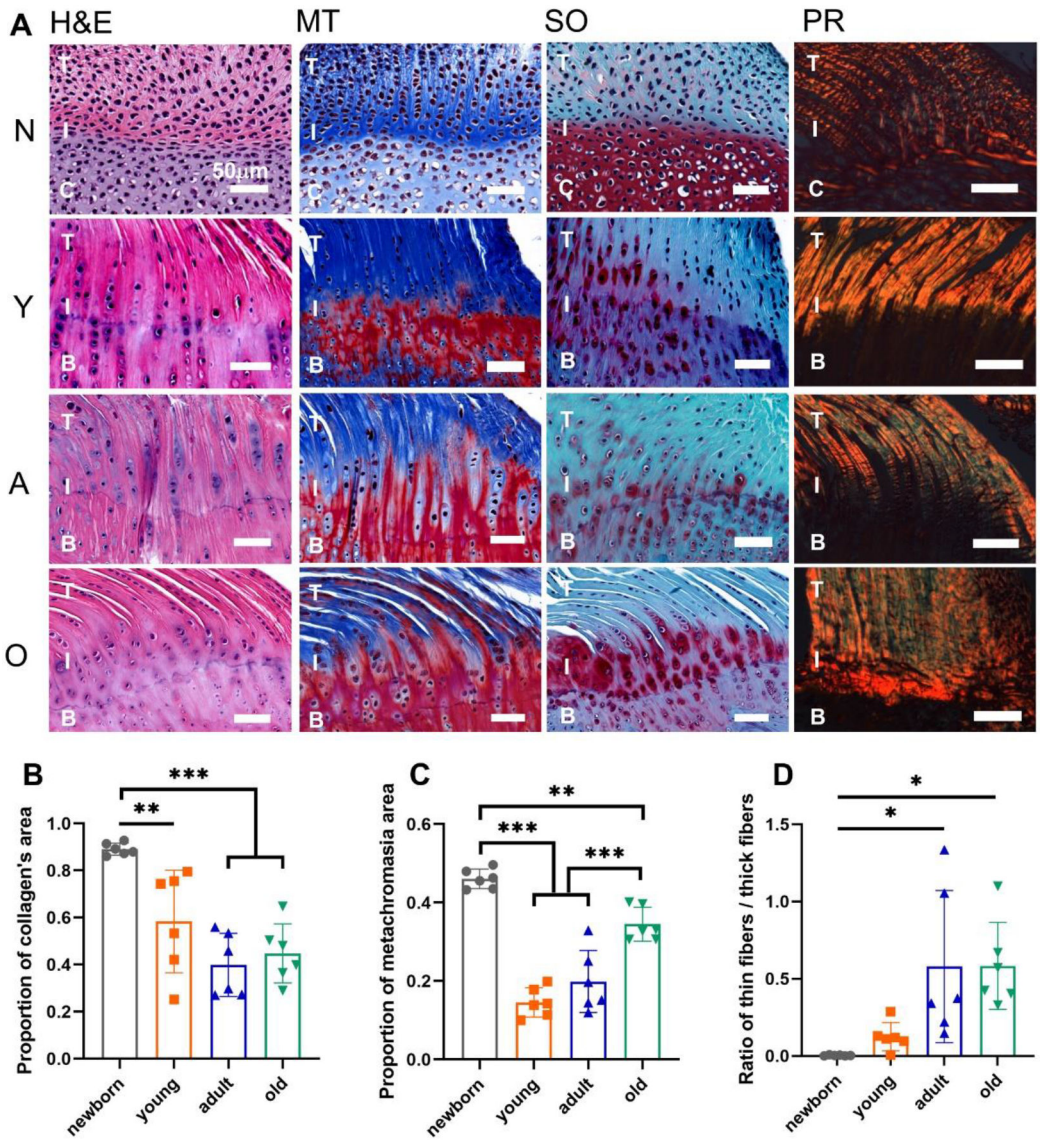

Figure 2.

The histological staining and semi-quantification of the supraspinatus tendon-to-bone interface in four age groups. (A) The H&E, Masson's Trichrome (MT), Safranin O (SO), and Picrosirius red (PR) staining of the supraspinatus tendon-to-bone interface with the newborn (N), young (Y), adult (A), old (O) groups. (B) The proportion of collagen's area. (C) The proportion of metachromasia area. (D) The ratio of thin collagen fibers / thick collagen fibers. (T: tendon; C: cartilage; I: interface; B: bone; scale bar: 50 μm; n = 6, *p < 0.05, **p < 0.01, ***p < 0.001)

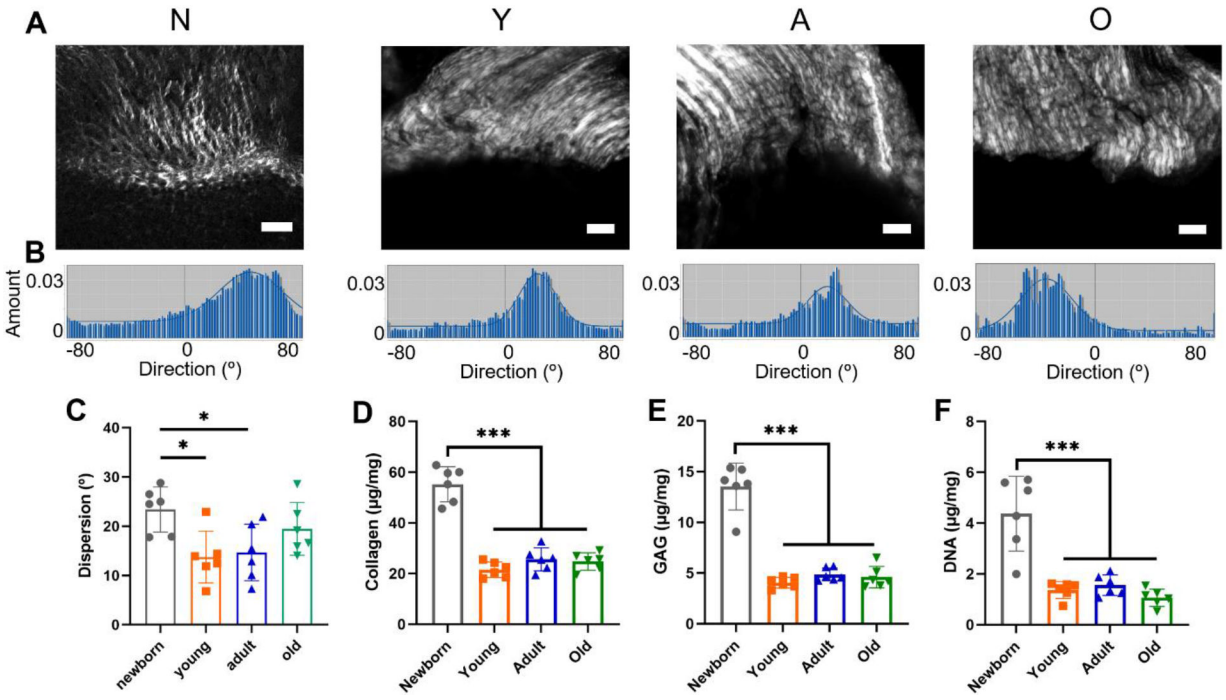

Figure 3.

The alterations of collagen fiber organization, collagen and GAG contents, and DNA content for the supraspinatus tendon-to-bone interface in the four age groups. (A) The SHG imaging of the supraspinatus enthesis with the newborn (N), young (Y), adult (A), and old (O) groups (Scale bar: 50 μm). (B) The representative dispersion graphs of the supraspinatus entheses for the four age groups. (C) The dispersion analysis of the supraspinatus entheses. (D) Collagen content analysis. (E) GAG content analysis. (F) DNA content analysis. (n = 6, *p < 0.05, **p < 0.01, ***p < 0.001)

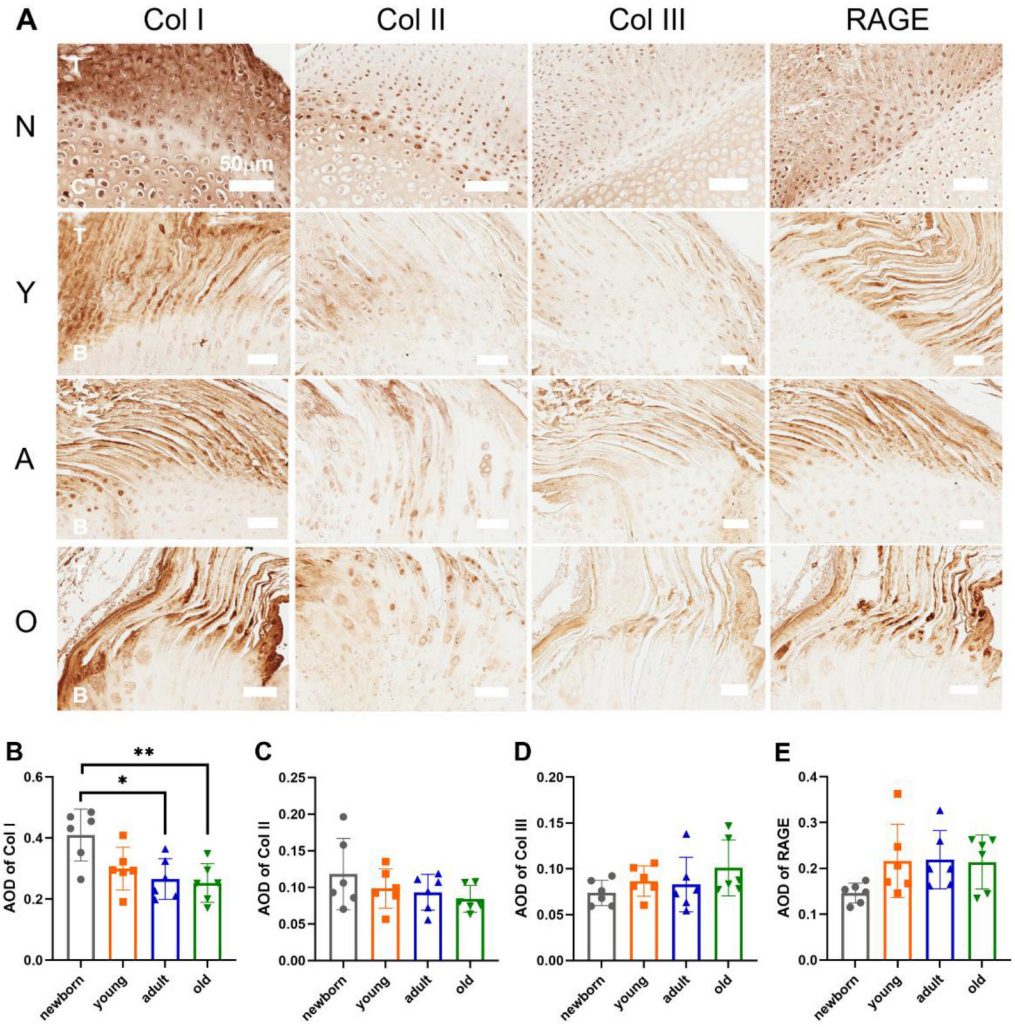

Figure 4.

IHC staining and analysis of types I, II, and III collagen and RAGE in the four age groups. (A) The IHC staining of types I, II, and III collagen and RAGE in the newborn (N), young (Y), adult (A), and old (O) groups (T: tendon; C: cartilage; B: bone; scale bar: 50μm). (B) Average optical density (AOD) of type I collagen. (C) AOD of type II collagen. (D) AOD of type III collagen. (E) AOD of RAGE. (n = 6, *p < 0.05, **p < 0.01, ***p < 0.001)

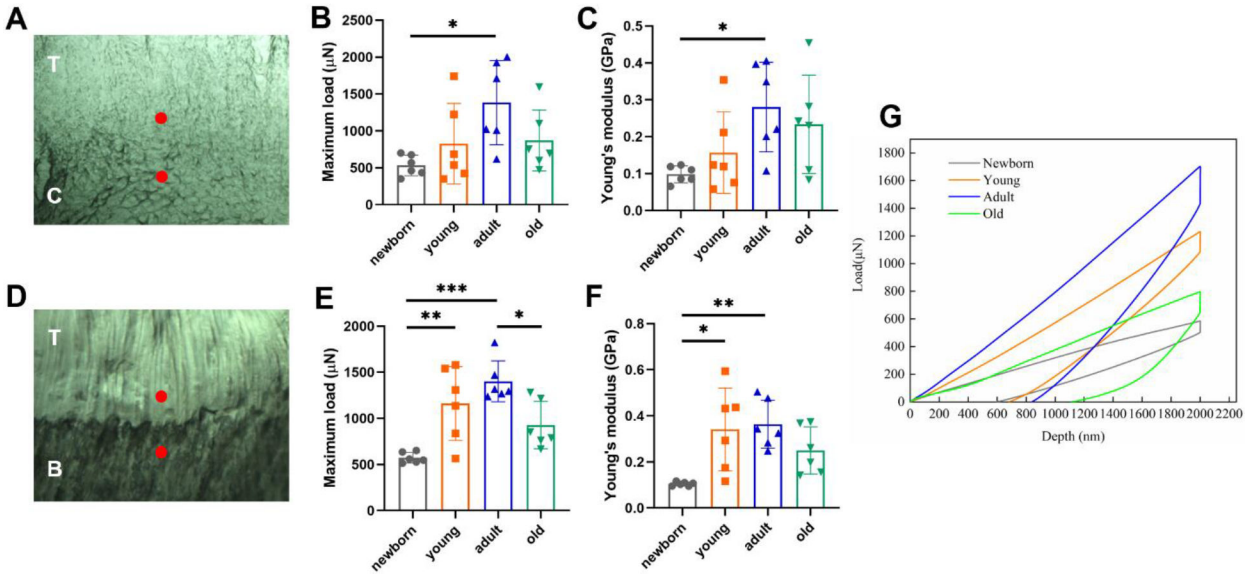

Figure 5.

Nanoindentation testing. (A, D) Indentation sites of the enthesis. A: upper red dot indicates the indentation region near the tendon and the lower red dot indicates the region near the cartilage in the newborn group (T: tendon; C: cartilage); D: upper red dot indicates the indentation region near the tendon and the lower red dot indicates the region near the bone in the in the young, adult, or old groups. (T: tendon; B: bone). (B) The maximum load of the enthesis near the tendon. (C) The Young's modulus of the enthesis near the tendon. (E) The maximum load of the enthesis near the cartilage/bone. (F) The Young's modulus of the enthesis near the cartilage/bone. (G) The representative load-depth curve for all four age groups.

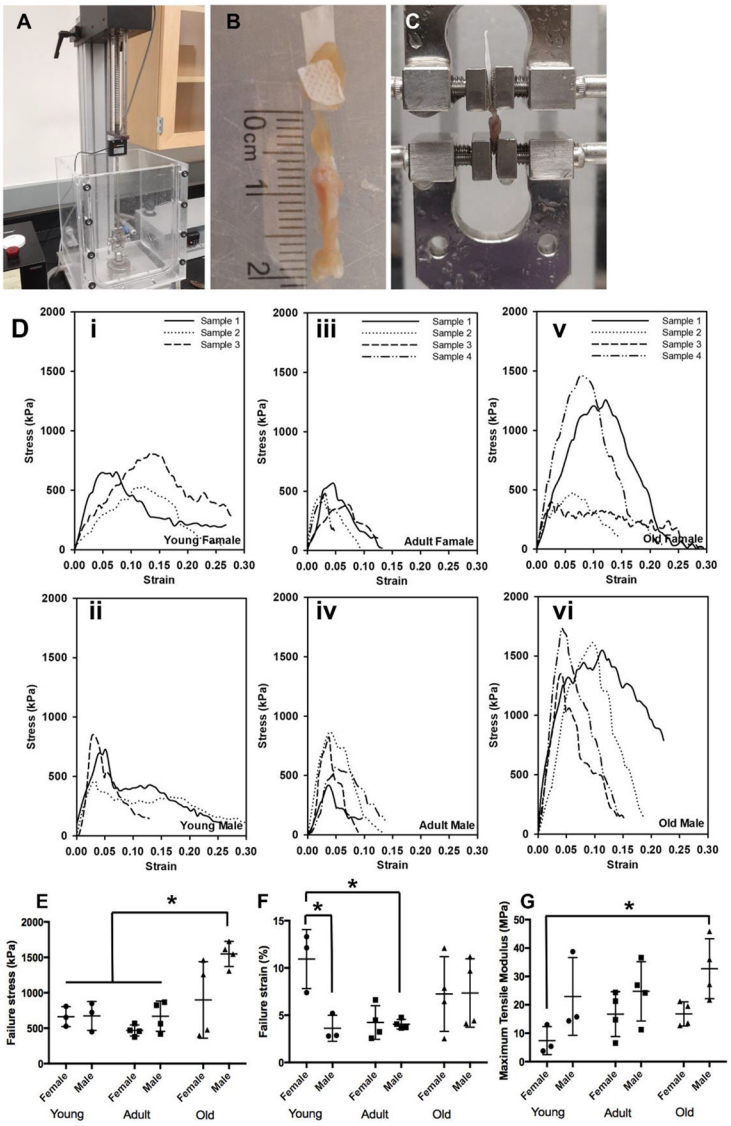

Figure 6.

Uniaxial mechanical characterizations. (A) Uniaxial mechanical testing device. (B) A sample was used for testing with a polymer wrap around the muscle part to achieve secure clamping. (C) Sample mounted for failure mechanical testing. (D) Failure stress-strain curves for (i) young female group, (ii) adult female group, (iii) old female group, (iv) young male group, (v) adult male group, and (vi) old male group. Comparisons of (E) failure stresses, (F) failure strains, and (G) maximum tensile moduli among the young female, young male, adult female, adult male, old female, and old male groups. (n = 3 for young male and young female groups, n = 4 for the adult male, adult female, old male, and old female groups, *$p < 0.05$)

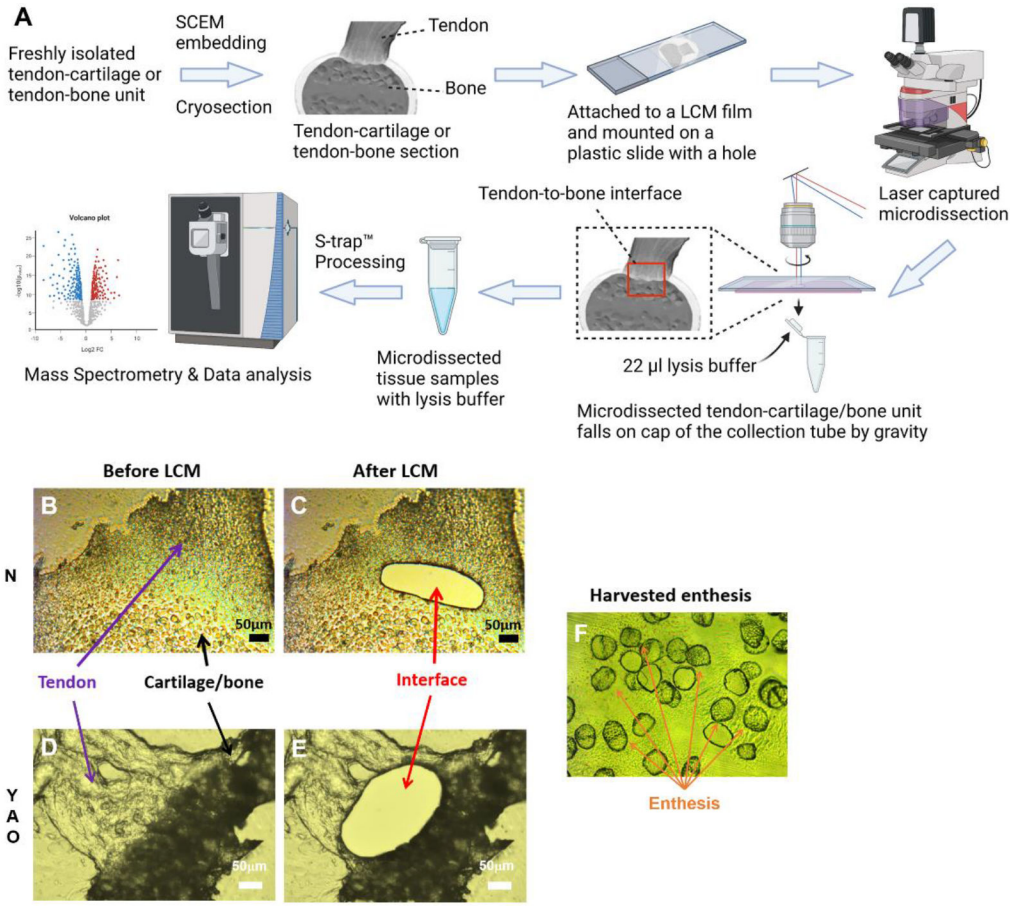

Figure 7.

Sample preparation for LC-MS and proteomics analysis. (A) The sample preparation workflow. Created with BioRender.com. (B) The image of the supraspinatus tendon and humerus cartilage with intact enthesis before LCM in the newborn group. (C) The image of the supraspinatus tendon and humerus cartilage with enthesis isolated after LCM in the newborn group. (D) The image of the supraspinatus tendon and humerus bone with intact enthesis before LCM in the young, adult, or old groups. (E) The supraspinatus tendon with humerus bone images with enthesis isolated after LCM in the young, adult, or old groups. (F) The isolated entheses in the cap of the PCR collecting tube. (Scale bar: 50 µm)

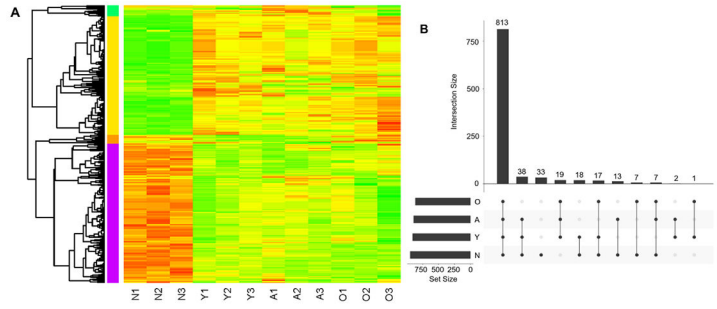

C

Lower abundance proteins (Y has less)	FC
Matrilin-1	0.006
Collagen alpha-1(XIV) chain	0.036
PAPS synthase 2	0.038
Prolyl 3-hydroxylase 2	0.040
Peptidyl-prolyl cis-trans isomerase FKBP10	0.056
Matrilin-4	0.057
Collagen alpha-1(IX) chain	0.075
Nervous system overexpressed protein 20	0.078
Obscurin-like protein 1	0.085
Endoplasmic reticulum protein SC65	0.094
Prolyl 3-hydroxylase 3	0.097
Procollagen galactosyltransferase 1	0.102
Procollagen-lysine,2-oxoglutarate 5-dioxygenase 2	0.103
Lamin-B1	0.108
Fibulin-4	0.111
Platelet-activating factor acetylhydrolase IB subunit alpha1	0.122
Cytoskeleton-associated protein 4	0.122
Elongator complex protein 3	0.127
Collagen alpha-2(XI) chain	0.128
Chondroadherin	0.131

Higher abundance proteins (Y has more)	FC
Microfibrillar-associated protein 5	57.673
Coagulation factor II	46.550
Neural cell adhesion molecule 2	35.127
Vitamin K-dependent protein S	28.395
Microsomal glutathione S-transferase 2	27.243
Alkaline phosphatase	23.159
Fibrillin-1	21.305
Superoxide dismutase [Cu-Zn]	18.135
Sarcoplasmic/endoplasmic reticulum calcium ATPase 1	17.950
Collagen alpha-2(I) chain	16.850
Apolipoprotein E	16.161
Ryanodine receptor 2	12.690
Prolargin	12.265
Protein-arginine deiminase type-2	12.078
Long-chain-fatty-acid--CoA ligase 1	11.443
Tropomyosin beta chain	10.988
Band 3 anion transport protein	10.805
Collagen alpha-1(I) chain	9.494
Dermatopontin	9.105
Ethylmalonyl-CoA decarboxylase	8.599

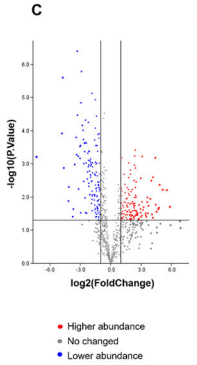

D

Lower abundance proteins (O has less)	FC
PDZ and LIM domain protein 7	0.086
Matrix metalloproteinase-9	0.175
CD177 antigen	0.204
GDP-L-fucose synthase	0.238
DNA replication licensing factor MCM2	0.243
Kazal-type serine protease inhibitor domain-containing protein 1	0.272
Fibulin-7	0.297
Nuclear pore complex protein Nup133	0.298
Epidermal growth factor receptor kinase substrate 8-like protein 2	0.303
Neprilysin	0.318
Nidogen-2	0.318
Inhibitor of carbonic anhydrase	0.373
Collagen alpha-2(XI) chain	0.380
Coagulation factor X	0.381
Thyroid hormone receptor-associated protein 3	0.398
Splicing factor 3B subunit 3	0.398
Alkaline phosphatase	0.421
Amyloid-beta A4 protein	0.426
Ribonucleoprotein PTB-binding 1	0.432
Tapasin	0.436

Higher abundance proteins (O has more)	FC
5'-3' exoribonuclease 2	6.379
Elastin	4.466
Glycerol-3-phosphate dehydrogenase	3.319
Apolipoprotein A-IV	3.272
Short-chain specific acyl-CoA dehydrogenase	3.158
Secretory phospholipase A2 receptor	2.929
Glycogen phosphorylase	2.566
Vacuolar protein sorting-associated protein 35	2.357
Long-chain specific acyl-CoA dehydrogenase	2.322
Vimentin	2.111
Glyceraldehyde-3-phosphate dehydrogenase	2.100
Kinesin-1 heavy chain	2.063
L-lactate dehydrogenase A chain	2.030

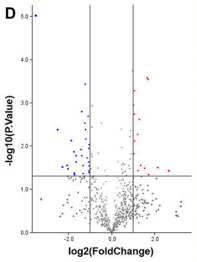

Figure 8.

Proteomics analysis. (A) The heatmap of the four age groups, with three biological replicates for each group. The proteins selected were based on a false discovery rate (FDR) < 0.05 and an absolute average log2 ratio > 1. (B) The UpSet plot of all the proteins identified for the four age groups. (C) The volcano plot of proteins in the young and newborn groups. The blue dots represent the lower abundance proteins in the young group compared to the newborn group. The red dots represent the higher abundance proteins in the young group compared to the newborn group. The gray dots show the proteins with no difference between the two groups. The top 20 lower and higher abundance proteins are listed (FC: fold change). (D) The volcano plot of proteins in the old and adult groups. The blue dots represent the lower abundance proteins in the old group compared to the adult group. The red dots represent the higher abundance proteins in the old group compared to the adult group. The gray dots show the proteins with no difference between the two groups. The top 20 lower abundance and top 20 higher abundance proteins are listed (FC: fold change).